Photoconductivity of crystalline anthracene induced by tunable dye lasers

Amalia Bergman and Joshua Jortner
Department of Chemistry, Tel-Aviv University, Tel-Aviv, Israel
(Received 29 June 1973)

We present the results of an experimental study of the bulk photoconductivity of crystalline anthracene induced by high-power ($I \simeq 10^{22}-10^{24}$-photon $cm^{-2}\,sec^{-1}$) tunable dye lasers in the wavelength region $\lambda = 6943$–4150 Å. The kinetic data for the dependence of the charge carrier density m on the excitation intensity I fall into three regions: (I) In the excitation region $\lambda = 6943$–6180 Å a $m \propto I^3$ dependence has been observed originating from photoionization of two-photon-excited singlet states. (II) In the range $\lambda = 6120$–4600 Å a complex, superlinear pattern was observed, exhibiting a $m \propto I^2$ dependence at low I and $m \propto I^4$ dependence at high I. In this range, where excitation occurs via two-photon absorption, three charge-carrier-generation processes involving autoionization of metastable excitons, exciton photoionization, and exciton-exciton collision ionization are operating. Detailed information was obtained regarding the energy dependence of the generation coefficients for these processes. (III) In the excitation range $\lambda = 4600$–4400 Å a $m \propto I^2$ dependence was observed and interpreted in terms of photoionization of one-photon-excited singlet states. From the generation coefficients in regions I and III and from the $m \propto I^3$ generation coefficient in region II, detailed information has been obtained regarding the energy dependence of the cross section for exciton photoionization. From the $m \propto I^4$ generation coefficient in region II we have obtained the rate coefficient $(4 \pm 2) \times 10^{-12}$ $cm^3\,sec^{-1}$ for the exciton collision ionization while the autoionization efficiency of metastable excitons produced by exciton collisions is $(7 \pm 4) \times 10^{-5}$. The two-photon-induced $m \propto I^2$ generation coefficients in region II, normalized by the two-photon-absorption cross sections, result in a detailed energy dependence of the autoionization efficiency $\eta(E)$. The direct onset to the conduction band is $E_g = 4.08 \pm 0.04$ eV. $\eta(E)$ yields a reasonable measure for the weighted density of states for interband transitions, providing experimental evidence for narrow (~ 1000-cm^{-1}) vibronic components of the valence and conduction band, which exhibit vibrational structure near the threshold.

I. INTRODUCTION

The understanding of charge-carrier generation in low-mobility materials is an interesting problem in solid-state physics. During the last decade there have been extensive experimental and theoretical investigations [1–6] of the photoconductivity of organic crystals, with crystalline anthracene providing a convenient prototype system for the elucidation of the energetic and dynamic processes involved in photogeneration of charge carriers in such systems.

In crystalline anthracene it has been conclusively demonstrated that in addition to the "conventional" intrinsic one-photon-induced charge-carrier-generation process, [7–9] two-photon excitation[10] provides a powerful tool for the study of novel and interesting mechanisms: (a) stable excitons can yield carriers by photoionization[11–13] or by exciton-collision processes[14,15] and (b) metastable excitons can decay by autoionization. [16–20] The two-photon excitation processes were studied up to date by utilizing Q-switched solid-state lasers in their fundamental, [12,13] second-harmonic, [19,20] and Raman-shifted[19] output. With the advent of high-power, continuously tunable dye lasers, the detailed energy dependence of various charge-carrier-generating mechanisms, resulting from two-photon (and one-photon) excitation, became amenable to direct study. In this paper we report the results of an experimental investigation of the bulk photoconductivity, induced in crystalline anthracene by a high-power dye laser. Intrinsic-charge-carrier generation, induced by weakly absorbed light in the bulk, was accomplished by two-photon absorption in the high-energy region ($\lambda = 4500$–7000 Å, $2h\nu = 28\,570$–$44\,440$ cm^{-1}) as well as by one-photon absorption in the low-energy Urbach-type absorption tail ($\lambda = 4150$–4500 Å, $h\nu = 44\,440$–$48\,200$ cm^{-1}).

II. REVIEW OF RELATIONSHIP BETWEEN ENERGY LEVELS AND PHOTOCONDUCTIVITY

Let us first consider the pertinent information regarding the crystal energy levels and the dyanmic processes involved in intrinsic charge carrier generation in organic crystals. A simplified energy level diagram of crystalline anthracene is portrayed in Fig. 1. As is well established, the lowest electronically excited states are reasonably well described within the tight-binding approximation. [21,22] The location of the Frenkel-Davydov exciton states was obtained from conventional one-photon spectroscopy[22] and from recent two-photon spectroscopy[23–29] of crystalline anthracene. We have also incorporated in this diagram some of the totally symmetric vibronic components of the neutral exciton states, which result in the conventional vibrational spread of those odd-parity exciton states which correspond to the weak exciton (intramolecular) vibrational coupling[30] limit and of all the

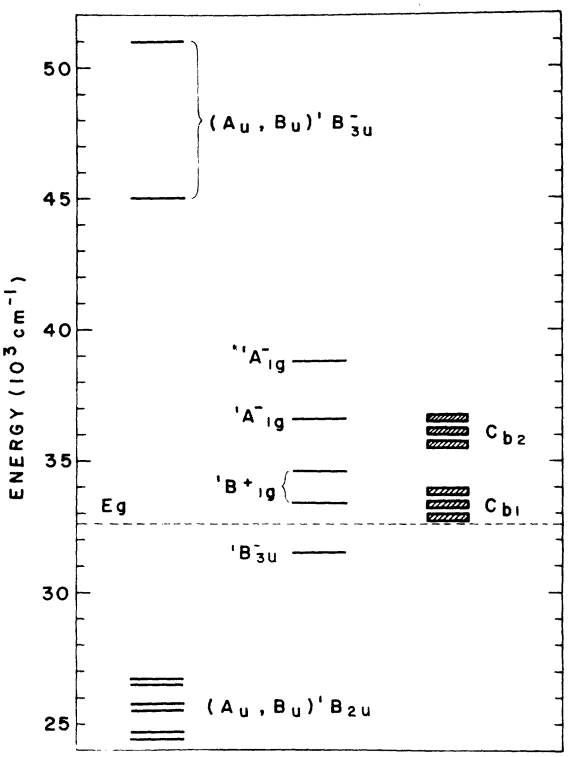

FIG. 1. Schematic energy level of crystalline anthracene.

even-parity exciton states.

In addition to Frenkel-type exciton states, the existence of charge-transfer excitons[28,31-36] was invoked for the interpretation of the Davydov splitting in triplet states, triplet-exciton progagation and recombination, and singlet-exciton fusion. To the best of our knowledge no direct experimental evidence is yet available for the location of these bound-charge-transfer states in organic crystals. Experimental photoemission data from crystalline anthracene,[35-37] excited in the energy region 4–5 eV, which were originally interpreted[35-37] in terms of mutual annihilation of two charge-transfer states located at 3.6 eV, result from exciton–charge-carrier interaction.[38] Also, the two-photon-excited state in the range 3.5–3.8 eV, which was tentatively assigned to a g-type charge-transfer state of the crystal,[28] was recently demonstrated[29] to originate from the vibronically induced $^1A_{1g}(A_g) \rightarrow {}^1B_{3u}(A_u, B_u)$ transition to a Frenkel state. Although these crystal charge-transfer Wannier-type states are probably important in configuration-interaction mixing, their relevance for the dynamics of charge-carrier production was not established, and we have refrained from including these states in the energy-level scheme.

We shall now turn to the valence- and the conduction-band states. The direct threshold to the conduction band, which corresponds to the bottom of the lowest conduction band relative to the ground state of the crystal, was experimentally determined from one-photon intrinsic photoconductivity[5,7-9] and from photoinjection studies[39] to be located at 3.9 ± 0.1 eV. The pioneering theoretical study of Leblanc[40] has demonstrated that the highest valence band and the lowest conduction band are quite narrow (bandwidth $\sim 0.01-0.05$ eV). These bands were constructed within the framework of the tight-binding approximation utilizing the highest filled and the lowest empty molecular orbitals as proper basis sets and invoking the intermolecular Coulomb interactions. Subsequent studies[41-43] incorporated the role of intermolecular exchange interactions[42] and long-range polarization interactions,[43] which did not, however, grossly modify the bandwidths. More important, it was pointed out[42] that as the width of the conduction and the valence bands is small, relative to the intramolecular vibrational frequency, the weak electron-vibrational coupling limit is applicable. The bands will exhibit vibrational splitting, the width of each vibronic valence band and vibronic conduction band will be proportional to an appropriate Franck-Condon type nuclear overlap integral. Thus each narrow band corresponding to a single electronic configuration will exhibit vibrational splitting. Furthermore, the (vibronically split) conduction and valence bands explicitly considered by Leblanc[40] and others[41-43] are by no means the only free electron and hole states of the crystal. Lower lying valence bands and higher conduction bands originate from the corresponding lower filled and from the higher empty molecular orbitals, respectively, each of which will also exhibit vibrational splitting. In Fig. 1 we have displayed schematically these bands, utilizing just a single, totally symmetrical, vibration. Some evidence for the vibrational structure of the lowest conduction band has been obtained from photoinjection experiments,[39] while conclusive evidence for electronic splitting resulting in "higher" conduction and valence bands which originate from different electronic configurations was obtained from one-photon photoconductivity,[18] energy resolved photoemission,[44] and photoinjection[39,45] studies. From the foregoing considerations it is evident that the naive description of organic crystals in terms of "narrow" conduction and valence bands should be grossly modified in view of the vibrational splitting and the multitude of vibronic bands originating from different electronic configurations. Thus, just above the threshold for the lowest interband separation vibrational structure will be exhibited, while at somewhat higher energies congestion of higher bands will be encountered and even this vibrational sturcture will be washed out.

The Frenkel exciton states and the (conduction and valence) band states constitute the zero-order levels of the system. Coulomb interactions couple the exciton and band states, nonadiabatic intramolecular terms couple vibronic components of exciton states which correspond to different electronic configurations, while nuclear coupling terms involving both intermolecular and intramolecular nuclear displacements will couple different vibronic components of a single electronic configuration of either a neutral exciton or a band state. Thus several kinds of nonradiative decay processes are expected to occur. For exciton states located below the lowest interband gap (i.e., below 4 eV) two such processes should be considered: (a) vibrational relaxation within a single electronic manifold; (b) electronic relaxation between different electronic states.[17,46]

Internal conversion[46] between high excited electronic states of a large molecule is characterized by relaxation times shorter than $\sim 10^{-11}$ sec (for high excited states this relaxation time was estimated[17] to be 10^{-14} sec). The vibrational relaxation processes in electronically excited states of large molecular occurs on the time scale of $\sim 10^{-11}$–10^{-12} sec. Disregarding intersystem crossing to the triplet state, then the lowest excited singlet state of crystalline anthracene vibrational relaxation prevails. In higher excited states electronic relaxation of the "initially excited" high state (which carries the oscillator strength from the ground state) simultaneously with vibrational relaxation both in the initial and final electronic manifolds occur. It is well known[46] that vibrational relaxation in the final electronic manifold does not affect the characteristics of the nonradiative decay pattern in large molecules. As internal conversion from high singlet states is efficient on the time scale of their radiative decay vibrational relaxation in the final manifold will result in a thermal population of the low vibronic components of the first excited singlet state. When the energy increases above the conduction band a new decay mechanism sets in.

(c) Exciton states located above the direct threshold to the conduction band are metastable with respect to autoionization and to internal conversion,[16–18] whereupon these Frenkel-type zero-order excited states will exhibit parallel decay into two open channels.

The formal description of the autoionization process has been previously presented in relation to exciton collision ionization.[17] We shall now present a reformulation of the problem in relation to autoionization resulting from one-[18] or two-photon optical excitation.[47] The wave function ψ_E of the metastable state resulting from a single resonance can be recast in terms of the Fano configuration-interaction method,[48]

$$\psi_E = a(E)\phi + \sum_i b_i \phi_i + \int C_{E'} \phi_{E'} \rho(E') dE' \qquad (1)$$

where $\{\phi_{E'}\}$ are the crystal uncorrelated electron-hole conducting states represented by the density of states $\rho(E')$. This density of states corresponds to the weighted density of states in the valence and in the conduction band. $\{\phi_i\}$ represents the dense manifold of the intramolecular vibronic states which corresponds to a lower electronic configuration and which are characterized by a density of states ρ_i. It is well established that the vibronic manifold $\{\phi_i\}$ does not carry oscillator strength for one photon or for multiphoton transitions from the ground state. We shall further assume that the optical transition strength from the ground state ϕ_g to the conduction band is weak relative to the transition to the (zero-order) bound-exciton state. This assumption rests on three experimental facts. First, in the optical one- and two-photon spectra of crystalline anthracene no evidence was ever obtained for Fano-type antiresonances in the optical line shapes[17] which indicate that the transition moment for direct transitions to the conduction band is small. Second, theoretical estimates of the oscillator strength for interband transition[49] results in low values for this quantity. Third, the low yield $\sim 10^{-4}$ for charge carrier production via singlet-exciton collisions[6,17,50] and by two-photon absorption[6] seems to support this conclusion. We thus set $\langle \phi_g | M | \phi \rangle \neq 0$, while $\langle \phi_g | M | \phi_i \rangle \rho_i \simeq 0$ and $\langle \phi_g | M | \phi_E \rangle \rho(E) = 0$, where the generalized transition moment M for one-photon excitation corresponds just to the ordinary dipole operator, while for two-photon transitions M is the Gouppert-Meyer second-order perturbation sum[10] of transition moments via intermediate states divided by the appropriate energy denominators. The line shape $L(E)$ at excitation energy E is now given for a single resonance in terms of a Lorentzian,[17,48]

$$L(E) = \frac{(W_E + J_E)|M|^2}{(E - E_\phi)^2 + (W_E + J_E)^2}, \qquad (2)$$

where the partial half-width for the panarel decay of ϕ into the intramolecular manifold and into the conduction band are

$$J_E = \pi |\langle \phi_E | H | \phi \rangle|^2 \rho(E) \equiv \pi |V_E|^2 \rho(E), \qquad (3a)$$

$$W_E = \pi |\langle \phi_i | H | \phi \rangle|^2 \rho_i . \qquad (3b)$$

We now consider weak light absorption, as is always the case for two photon excitation. Further, we assert that the decay rate of $\phi = \hbar/(J_E + W_E)$ is fast on the time scale of vibrational relaxation in the initial electronic state. The efficiency of charge carrier generation $\varphi(E)$ at excitation energy E, is then expressed in terms of the product of the

line-shape function (2) and the autoionization yield

$$\varphi(E) = L(E)[J_E/(J_E + W_E)] \ . \tag{4}$$

Finally, on the basis of previous theoretical analysis and experimental data the decay rate is dominated by electronic relaxation, i.e., $I_E/W_E \ll 1$, and one gets

$$\varphi(E) = L(E)(J_E/W_E) \ , \tag{4a}$$

whereupon the yield for charge carrier generation is

$$\overline{\eta}(E) = \varphi(E)/L(E) = J_E/W_E \ . \tag{5}$$

Equations (2)–(5) consider the single case of a single resonance. Provided that interference effects between zero-order bound states[46] are negligible, we can directly apply this formalism to a real crystal where $L(E)$ now corresponds to the actual optical line shape (i.e., the energy-dependent one- or two-photon absorption cross sections). Thus $\overline{\eta}(E)$ monitors energy dependence of the ratio I_E/W_E. Provided that the coupling matrix element $|V_E|$ and the width W_E are weakly varying with energy, then $\overline{\eta}(E)$ provides a measure of the weighted density of states $\rho(E)$ in the conduction band. Such an assumption can be invoked only for a narrow energy region, where we hopefully can obtain some rough information regarding the energy dependence of the density of states in the conduction band.

It is important to point out that in organic crystals one cannot separate direct transitions to the conduction band from autoionization processes. The crystal resonance states (above the interband threshold) constitute an admixture of (zero-order) exciton states and conduction-band states and the whole energy region is spanned by these resonances, which include a major contribution from the bound states. Only in spectral regions where the contribution from the continuum states dominates the optical absorption is it legitimate to consider charge-carrier generation via direct interband transitions. Such a physical situation does not prevail in organic crystals.

Finally, we have to consider the relation between the theoretical autoionization yield $\overline{\eta}(E)$, Eq. (5), and the experimental yield $\eta(E)$ for charge carrier generation. Experimental studies[51(a)–51(e)] of the electric field and temperature dependence of the quantum yields for one-photon induced charge carrier generation in crystalline anthracene have established the important role of electron-hole geminate recombination on $\eta(E)$. Thus the experimental low-field quantum yield represents the residual autoionization yield of charge carriers, initially produced by autoionization, which subsequently escape geminate recombination. The attentuation of the experimental residual yield $\eta(E)$ relative to primary autoionization yield $\langle\overline{\eta}(E)\rangle$ may be energy dependent. To explore this point we recall that Onsager's theory[51(b),51(f)] results in the following approximate relation for the quantum yield at weak electric fields:

$$\eta(E) = \overline{\eta}(E)e^{-\lambda/R_0(E)} \ , \tag{6}$$

where $\lambda = e^2/DRT$ is the characteristic thermal capture length, D being the dielectric constant. For crystalline anthracene, $D = 3.02$ and $\lambda = 192$ Å. $R_0(E)$ represents the energy-dependent pair separation length. The one-photon data of Batt *et al.*[51(b)] demonstrate that $R_0(E)$ is practically constant in the energy range 4.2–5.1 eV, where $\eta(E)/\overline{\eta}(E) = \exp(-192/80) = 0.09$, while at 6.1 eV, $\eta(E)/\overline{\eta}(E) = \exp(-192/110) = 0.18$. Thus the experimental low-field quantum yield is attentuated by a factor 11–5.5 over the relevant energy range. It is important to notice that the attentuation factor $\exp[-\lambda/R_0(E)]$ exhibits a rather weak energy dependence. We can assert that the experimental values of the residual autoionization yields over the energy range 4.2–6.1 eV still provide a reasonable estimate of the relative values of the direct autoionization yield $\overline{\eta}(E)$, and will thus result in a measure of the weighted density of states in the conduction band.

To conclude this discussion we have summarized in Fig. 2 the relevant decay processes of a single excited state. Three further processes involving conduction-band states have been incorporated:

(d) An electron in a higher band can decay nonradiatively by vibrational relaxation to lower vibronic bands of the same electronic state in analogy to exciton vibrational relaxation [process (a)].

(e) A conduction band state originating from a

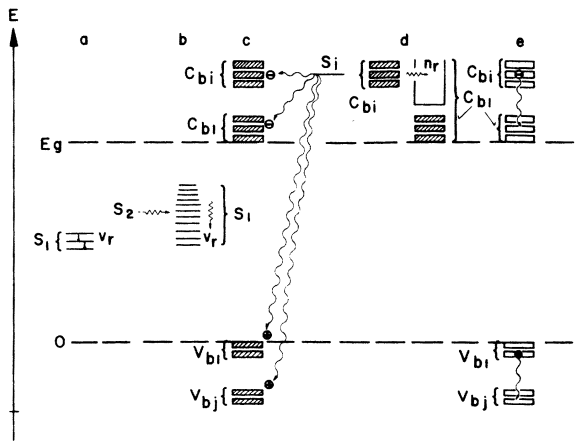

FIG. 2. Decay processes of singlet excited state: (a) vibrational relaxation; (b) electronic relaxation of excitons (followed by V_2); (c) autoionization of metastable excitons; (d) electronic relaxation between cb; (e) Auger decay. O ground state; E_g, direct threshold; S_i, Frenkel exciton state; V_{bi}, valence bands; C_{bj}, conduction bands.

high electronic configuration can decay nonradiatively to high vibronic levels of conduction bands which correspond to a lower electronic configuration, in analogy with exciton electronic relaxation process (b).

(f) If a hole is produced in a low-lying conduction band an Auger-type process can occur, where the hole is filled up from a higher valence band. These three processes were not yet studied in any detail.

Several mechanisms were advanced for intrinsic charge carrier generation in organic crystals. For excited states located below the direct threshold to the conduction-band the following indirect processes, overcoming the energy balance problem, should be considered.

(i) *Exciton photoionization.* Vibrationally relaxed singlet excitons S_1 at ~3.1 eV are optically excited to a metastable state A, which yields charge carrier $(e+h)$ via autoionization, with this decay process competing with internal conversion back to S_1 [6,11-13]:

$$S_0 \xrightarrow{h\nu \text{ or } 2h\nu} S_1 \xrightarrow{h\nu} A \begin{cases} \longrightarrow e+h \\ \longrightarrow S_1 \end{cases} .$$

This mechanism was demonstrated to provide the main pathway for the production of charge carriers by photoionization of two-photon-excited states[12,13] at 6943 Å, of one-photon-excited states at 4250 Å following subsequent photoionization at 5300 Å, [6] and also of consecutive photoionization of one-photon-excited states[19] at 4210 Å and at 4670 Å. It also appears that the experiments of Silver *et al.*[52] which were interpreted in terms of exciton collisions[14,17] are quantitatively explained[6] by this mechanism.

(ii) *Exciton collision ionization.* Vibrationally relaxed singlet excitons collide at a rate[50] $\gamma_s \simeq (6 \pm 2) \times 10^{-8}$ cm^3 sec^{-1}, yielding a metastable state A which decays by internal conversion back to S_1 or by autoionization[14-17]:

$$S_0 \xrightarrow{h\nu \text{ or } 2h\nu} S_1 ,$$

$$2S_1 \longrightarrow A \begin{cases} \longrightarrow e+h \\ \longrightarrow S_1 \end{cases} .$$

Charge-carrier generation via one-photon excitation in the wavelength region 3300 Å–4000 Å was interpreted by Braun[15] in terms of this mechanism. The rate constant for collision ionization was found to be[15] $\gamma_c = 10^{-12}$ cm^2 sec, so that the branching ratio for the autoionization of A is[15] $\eta \sim \gamma_c/\gamma_s \sim 10^{-4}$. Some further evidence for this mechanism was obtained from photoemission studies[35,36] following excitation below 4 eV. It appears that up to date no observation of carrier generation resulting from collision ionization of two photon excited states has been reported. Such information is of interest as its intensity dependence will provide direct evidence for the validity of this interesting mechanism.

For metastable excitons located above 4 eV of the following charge generation mechanisms should be considered.

(iii) *Exciton autoionization.* Following our previous discussion in organic crystals one should consider the decay of metastable A states to the conduction band:

$$S_0 \xrightarrow{h\nu \text{ or } 2h\nu} A \begin{cases} \longrightarrow e+h \\ \longrightarrow S_1 \end{cases} .$$

One-photon-excitation experiments[7-9] established that this direct process occurs above 4 eV with a quantum yield $\eta \sim 10^{-4}$ in the region 3100 Å-2000 Å. Utilizing anti-Stokes Raman emission induced by a Q-switched ruby laser and the second harmonic of neodynium, Strome[19] and Kepler[6] have observed a direct two-photon-induced charge-carrier generation for excitations at 5970, 5710, 5300, and 5250 Å, which account for mechanism (3).

In view of the experimental low quantum efficiency[6,17] ($\eta \sim 10^{-4}$) for the carrier generation process the S_1 state resulting from internal conversion of A can further contribute to the charge carrier production via the indirect processes (i) and (ii). This effect was not exhibited in the previous results of Strome[19] and of Kepler, [6] who utilized relatively low ($I < 10^{23}$ photon cm^{-1} sec^{-1}) intensities.

III. EXPERIMENTAL PROCEDURES

The experimental set-up is presented in Fig. 3. A high purity, zone refined, single crystal of anthracene, dimensions (5×2×6 mm), with a vacuum deposited silver electrode on one end face and a silver-paint electrode at the other end was irradiated with a tunable dye laser perpendicular to the *ab* cleavage plane of the crystal.

The silver-paint electrode was made positive (1500 V) and the other electrode was connected to a matched 50-Ω line. The current was preamplified by a home made current amplifier which is characterized by a current gain factor of 6×10^5 and frequency bandwidth of 500 khz. The signal from the preamplifier was amplified by a HP 462A amplifier and displayed through a 50-Ω line on a Tektronix 454 oscilloscope. In order to obtain better results and to eliminate high-frequency noise we have added an RC integration circuit ($R = 1$ kΩ, $C = 1500$ pF). The electrode materials and polarities were chosen to avoid space charge effects. Special care was exerted to mask the electrodes for the laser beam.

The set-up of the tunable dye laser is described in Fig. 3. A 2-cm optical cell containing the dye solution was placed in a 6.5-cm resonant cavity formed by a Bausch and Lomb diffraction grating (600 groves/mm blazed at 5000 Å) and a dielectrically coated mirror (30% reflection over the

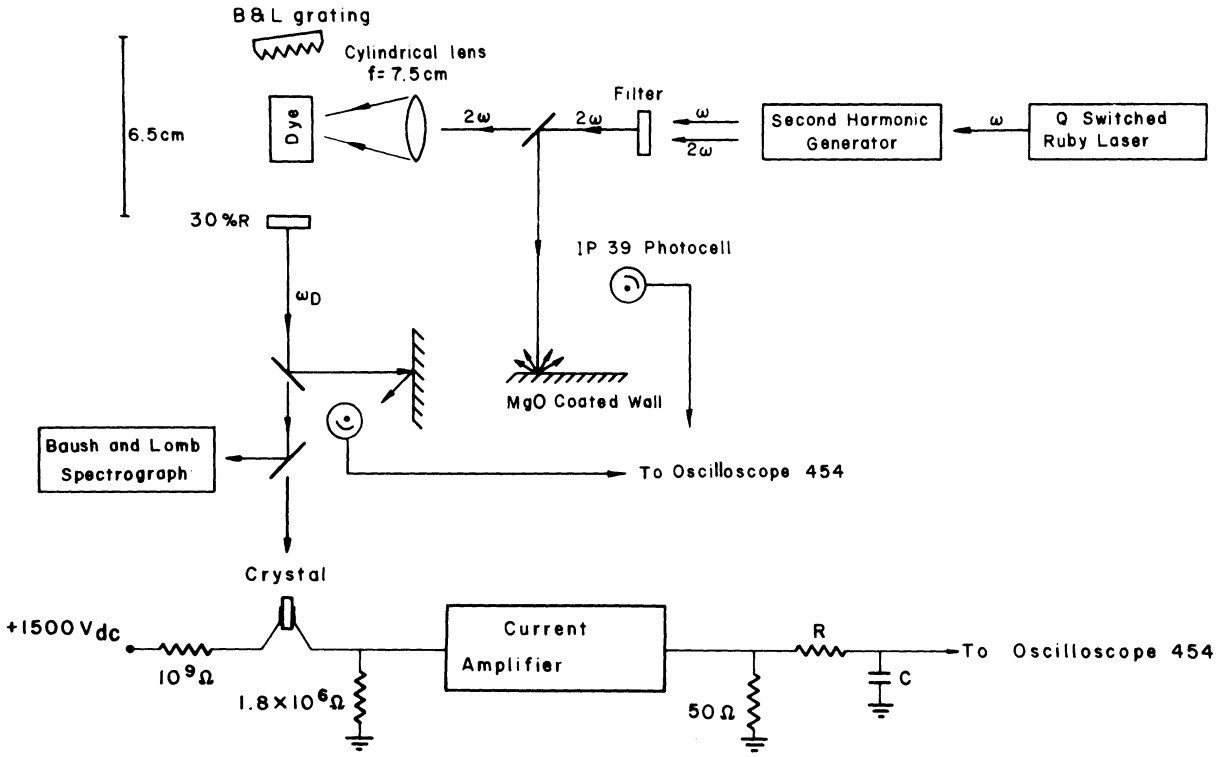

FIG. 3. Experimental set-up.

visible region). The grating was placed in a littrow mounting so that the light at a given tuned wavelength was reflected back along the axis of the cavity.

The pumping of the dye was performed with the second harmonic of a (cryptocyanine) Q-switched giant-pulse ruby laser. The 3472-Å pulse was characterized by a power of 1 MW and a pulse length of 20 nsec. It was focused with a cylindrical lens into the dye cell which was pumped transversally. In order to avoid channeled spectra the dye cell was placed in a Brewster angle. The intensity of the (unfocused) beam of the dye laser was determined by reflecting a small portion of the beam by a 45° glass plate on a diffusively scattering surface, followed by monitoring with a S/4-IP-39 photocell and a Tektronix 454 oscilloscope. The output wavelength of the tuned dye lasers was checked by photographing the spectrum with a Bausch and Lomb 1.5-m grating spectrograph employing 1000ASA, 35-mm Agfa film. The output of the (unfocused) dye lasers for a pumping power of 0.5 MW was: 75 kw for 4 methylumbelliferone (MU)-$HClO_4$,[53,54] 75 kw for Rhodamine 6G and 40 kw for Rhodamine B. The dye-laser pulse length was $\tau \simeq 10$–15 nsec. The tunability ranges of the dye lasers employed in this work are as follows: 4MU-$HClO_4$ ($10^{-2}M$ 4MU–$3M$ $HClO_4$ in ethanol) 4000–5000 Å, ($10^{-2}M$ 4MU–$1M$ $HClO_4$ in ethanol) 4650–5650 Å, Rhodamine 6G ($5\times10^{-4}M$ in ethanol) 5700–6300 Å and Rhodamine B ($10^{-3}M$ in ethanol) 6200–6500 Å. The spectral width of the pulse was 10 Å. Additional data were obtained at 6943 Å using the first harmonic of the ruby laser. The dye-laser beam was focused on the crystal by a 15-cm lens, and the light intensities thus obtained were in the range 10^{22}–10^{24} photons cm^{-2} sec^{-1}. The light intensity was controlled by attentuation with neutral density filters.

Typical response curves of the system are presented in Fig. 4. The current, displayed at the bottom of Fig. 4, increases downwards from the central line. The current overshoot is due to the integration circuit. The integration circuit does not modify the peak current. We have checked the current shape at high laser intensities ($\sim 10^{24}$ photon cm^{-2} sec^{-1}) without the integration circuit, where the overshoot was eliminated from the current curve. The current peak intensity was not affected by the integration circuit. The density m of electron-hole pairs was obtained from the peak of the photocurrent i by the relation: $i = m\mu eES$ where S is the electrode contact area and E is the electric field, μ is the mobility sum ($\mu_e + \mu_h$) which was taken[13] as 1.2 cm^2 V^{-1} sec^{-1}. The results obtained at 6943 Å excitation exhibited the $m \propto I^3$ dependence,

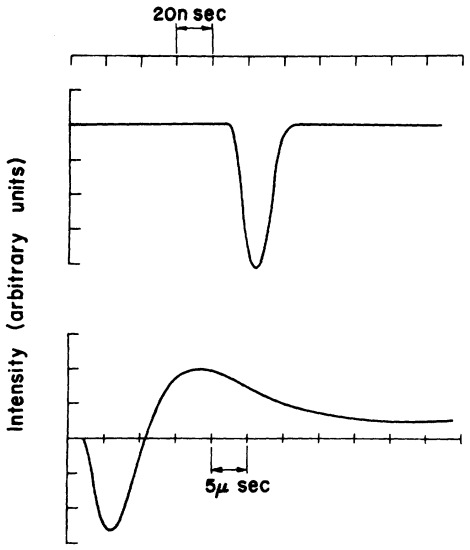

FIG. 4. Example of pulses obtained. Top, dye laser and bottom, photocurrent. The time scale was 20 nsec division (top) and 5 μsec (bottom). Current increasing downward from central line. The overshoot is due to integration circuit.

in agreement with the original data. We have obtained $m/I^3 = K_3 = 5\times10^{-65}$ cm^3 sec^3 photon^{-2} in accordance with the previous result[13,12] ($K_3 = 10^{-65}$ cm^3 sec^3 photon^{-2}). The charge carriers densities obtained herein were in the region 10^7–10^{10} cm^{-3}. Under these conditions charge-carrier recombinations (characterized by the rate 5×10^{-7} cm^3 sec^{-1}) are negligible.[13]

IV. EXPERIMENTAL RESULTS

A. Intensity dependence of charge carrier generation at different energies

The intensity dependence of intrinsic charge carrier generation in crystalline anthracene was studied in the excitation wavelength region 6943–4400 Å. Optical excitation mechanisms naturally fall into two categories.

(i) In the wavelength region 6943–4600 Å ($h\nu$ = 14 400–21 700 cm^{-1}) two-photon excitation takes place. The energy dependence of the two-photon absorption cross sections was studied by several groups[19,26,28] and recently we have obtained a detailed two-photon absorption spectrum of the crystal in the energy range $2h\nu$ = 28 800–46 000 cm^{-1}.[29]

(ii) In the wavelength region 4600–4400 Å one-photon excitation into the Urbach type exponential absorption tail occurs, the absorption coefficient at $T = 300\,^\circ$K being $\alpha = 10^{-3}$ cm^{-1} at 4500 Å and $\alpha = 8\times10^{-3}$ cm^{-1} at 4400 Å.[56]

Plots of the dependence of the peak charge-carriers density m on the dye-laser excitation intensity I are displayed in Fig. 5. Our experimental results fall into three regions, each exhibiting a different m-vs-I dependence.

(I) In the excitation wavelength region 6943–6180 Å we have observed a cubic dependence of the charge-carrier density on the laser-peak intensity. The $m \propto I^3$ at 6943 Å was originally reported by Kepler[12] and by Courtens *et al.*[13] In this wavelength region optical excitation occurs exclusively via two-photon absorption. Thus, our experimental data in region I are interpreted in terms of charge-carrier generation by photoionization of two-photon excited singlet exciton states (first mechanism in Sec. II).

(II) In the wavelength region 6120–4600 Å we have observed a complex superlinear m-vs-I dependence. For high light intensities ($I \sim 10^{24}$ photon cm^{-2} sec^{-1}) we have found a fourth-power dependence of m on I, while for lower intensities ($I \sim 10^{22}$–10^{23} photon cm^{-2} sec^{-1}) a $m \propto I^2$ dependence is exhibited. The square dependence for the lower intensities concurs with the previous experimental results for $I = 10^{22}$–10^{23} photon cm^{-2} sec^{-1} of Strome[19] at 5250, 5710, and 5970 Å and of Kepler[6] at 5259 Å.

In this region excitation occurs predominantly by two-photon absorption. The linear m-vs-I^2 dependence in the lower intensity region is assigned to autoionization of metastable excitons.[55] The $m \propto I^4$ dependence for high intensities originates from collision ionization (second mechanism in Sec. II) of S_1 stable excitons produced by intramolecular internal conversion. The compound m-vs-I dependence in this region can also contain a $m \propto I^3$ component from the photoionization of S_1 stable singlet excitons produced again by radiationless decay.

(III) For excitation wavelengths in the region 4600–4400 Å ($h\nu$ = 21 700–23 000 cm^{-1}) a linear dependence of m-vs-I^2 was observed over the intensity region. These results for this region concur with the observations of Strome,[19] and were included here for the sake of completeness. One photon excitation of S_1 predominates in this region. Following previous work it is evident that here charge carrier generation originates from either exciton photoionization or from exciton collisions of one-photon-excited stable singlet excitons.[6,15,19]

We now proceed to a quantitative analysis of our experimental data.

B. Kinetic analysis of charge carrier generation via two-photon excited states

In the spectral region where optical excitation of spin-allowed states proceeds by two-photon absorption, the charge-carrier concentration m, at a given excitation energy $h\nu$, is given in general by a simultaneous contribution from the three generation processes discussed in Secs. II and IV A:

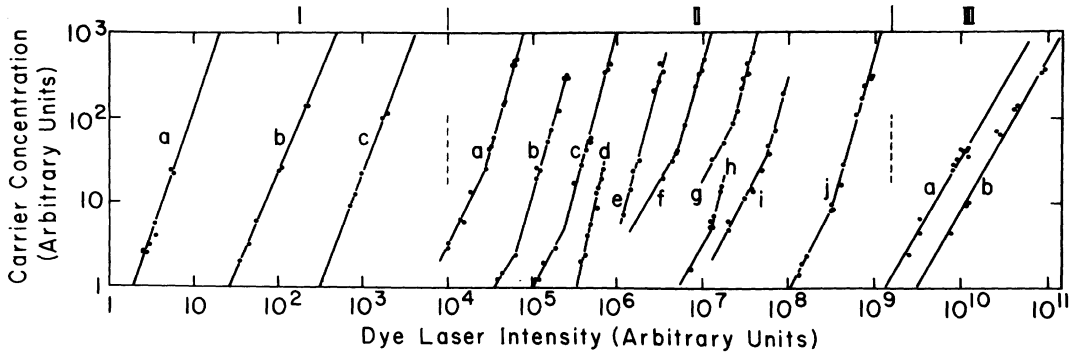

FIG. 5. Dependence of the peak charge-carrier density m on the dye laser excitation intensity I for various wavelengths.

		Wavelength λ (Å)	Units	Laser intensity I (photon cm^{-2} sec^{-1})	Carrier concentration m Units	cm^{-3}
I	(a)	6943	10	8×10^{24}	10	4.4×10^{9}
	(b)	6230	10^2	6×10^{23}	10	3×10^{8}
	(c)	6180	10^3	3×10^{22}	10	4×10^{7}
II	(a)	6120	10^4	2×10^{23}	1	10^{8}
	(b)	6050	10^5	2×10^{23}	10	1.5×10^{8}
	(c)	5990	10^5	10^{23}	10	4.4×10^{7}
	(d)	5530	5×10^5	3×10^{23}	60	4×10^{8}
	(e)	5460	2×10^6	10^{23}	60	10^{7}
	(f)	5250	6×10^6	4×10^{23}	10^2	10^{8}
	(g)	4930	10^7	1.4×10^{23}	20	10^{8}
	(h)	4880	10^7	1.5×10^{23}	3	3×10^{7}
	(i)	4740	2×10^7	8×10^{22}	50	10^{8}
	(j)	4670	10^8	10^{23}	1	10^{8}
III	(a)	4500	10^{10}	2×10^{24}	10	4×10^{10}
	(b)	4400	10^{10}	10^{23}	10	10^{9}

$$m = K_2(\nu)I^2(\nu) + K_3(\nu)I^3(\nu) + K_4(\nu)I^4(\nu) \ . \tag{7}$$

$K_2(\nu)$ is the generation coefficient via autoionization which is given by

$$K_2(\nu) = \sigma_2^c(2\nu)L\tau \ , \tag{8}$$

where τ is the length of the excitation pulse ($\tau = 10$–15 nsec), $L = 4.2\times10^{21}$ cm^{-3} is the number density, and $\sigma_2^c(2\nu)$ is the experimental cross section for charge carriers generation via autoionization at $2h\nu$.

$K_3(\nu)$ represents the generation coefficient for charge-carrier generation via exciton photoionization. We assume that under our experimental excitation condition electronic and vibrational relaxation times are exceedingly shorter than τ, whereupon ionization by a photon $h\nu$ occurs from the lowest S_1 exciton state at 3.1 eV. Thus we have

$$K_3(\nu)I^3(\nu) = \sigma_p(\nu)n_S\tau I \tag{9}$$

where $\sigma_p(\nu)$ is the cross section for S_1 exciton photoionization at $h\nu$. n_S represents the singlet exciton concentration. As the radiative decay rate of singlet excitons $\beta = 5\times10^7$ sec^{-1} is very close (within 50%) to τ^{-1} we set for two-photon excitations:

$$n_S = L\sigma_2^F(2\nu)I^2/\beta \ , \tag{10}$$

where σ_2^F is the two-photon-absorption coefficient at $2h\nu$. From Eqs. (9) and (10) we get

$$K_3(\nu) = \sigma_p(\nu)\sigma_2^F(2\nu)L\tau/\beta \ . \tag{11}$$

$K_4(\nu)$ corresponds to the generation coefficient for charge carriers via exciton collision ionization, from S_1 stable exciton states resulting from electronic and vibrational relaxation of higher stable or metastable excitons. A simple kinetic argument results in

$$K_4(\nu)I^4(\nu) = \gamma_c n_S^2\tau \ , \tag{12}$$

where γ_c is the collision ionization rate of a singlet pair (which is independent of ν). Utilizing Eq. (10) we have

$$K_4(\nu) = \gamma_c[L\sigma_2^F(2\nu)/\beta]\tau \ . \tag{13}$$

Equations (7), (8), (11), and (13) provide a complete kinetic picture of the relevant processes. From these results we arrive at the following conclusions.

(a) For excitation energies below the direct transition to the conduction band, E_g, the cross section via autoionization vanishes, i.e., $\sigma_2^c(2\nu) = 0$ for

$2h\nu < E_g$. Thus the onset of the $m \alpha I^2$ component in the yield signifies the onset of the conduction band.

(b) For $2h\nu < E_g$ the I^3 and I^4 components can contribute to charge-carrier generation. The ratio a for charge-carrier production via exciton photoionization and exciton collisions is

$$a = K_3(\nu)/K_4(\nu)I = \sigma_p(\nu)\beta/\gamma_c L \sigma_2^F I \,. \quad (14)$$

As tentative estimates we take the most favorable values $\gamma_c \simeq 10^{-11}$ cm^3 sec and $\sigma_p^c = 10^{-20}$ cm^2 and we get $a = 10^{-23}/\sigma_2^F I$. For relatively low $\sigma_2^F(2\nu)$ values $\sim 10^{-51}$–10^{-50} there is no hope of observing the contribution of the collision ionization process for $I < 10^{27}$ cm^{-2} sec^{-1}.

(c) From $K_3(\nu)$ and the independent $\sigma_2^F(2\nu)$ one can obtain the energy dependence of $\sigma_p(\nu)$. These data will result in the free carrier yield originating from autionization at the energy $E(S_1) + h\nu$.

(d) As γ_c in Eq. (13) is energy independent we expect that $K_4(\nu) \propto [\sigma_2^F(2\nu)]^2$, and from the two-photon-absorption spectra we can readily obtain a reliable value of γ_c.

The experimental results in region I correspond to $K_2 = 0$ and $K_4 = 0$. From the foregoing discussion it is obvious that here $2h\nu < E_g$. In view of the relatively low values of σ_2^F in this region (see Fig. 6) Eq. (14) yields $a < 10^{-2}$ for the highest light intensity achieved by us, so that the contribution of exciton collisions is negligible in accordance with the previous arguments of Courtens *et al.*[13] and by Schott.[57] The K_3 values obtained from the slopes in Fig. 5(I) are presented in Fig. 7.

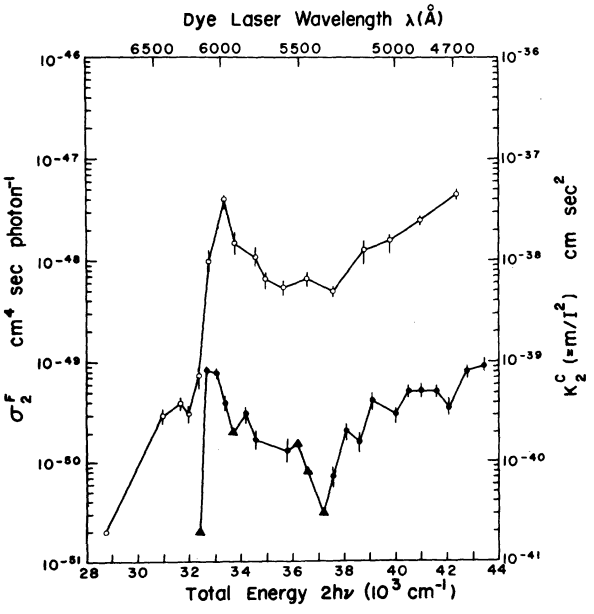

FIG. 6. Energy dependence of (a) two-photon absorption cross section σ_2^F, and (b) two-photon generation coefficient for charge carriers K_2^C. ▲, upper limit for K_2^C. O, experimental data for K_2^C from $M \propto I^2$ dependence at low I.

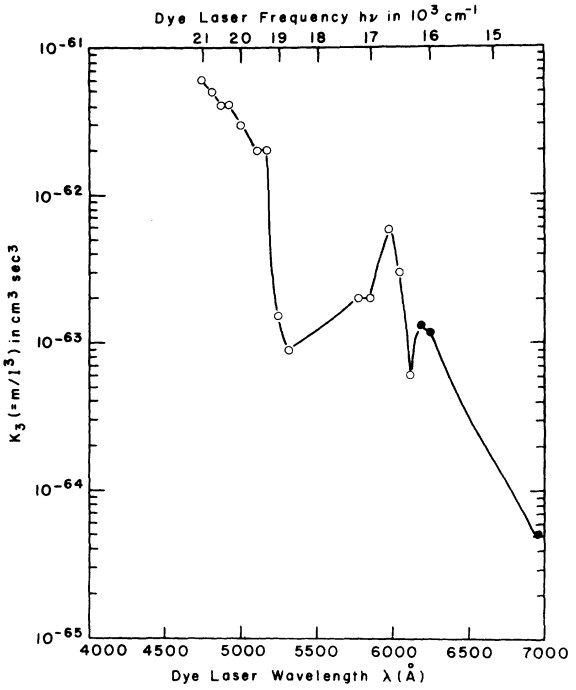

FIG. 7. Energy dependence of the generation coefficient for charge carrier generation via exciton photoionization, $K_2(\nu)$. ●, obtained from the slopes in Fig. 5(I); O, estimated values for K_3 in region II.

The compound intensity dependence of m in region II was analyzed according to Eq. (7). The K_2 values were obtained from the $m \propto I^2$ dependence in

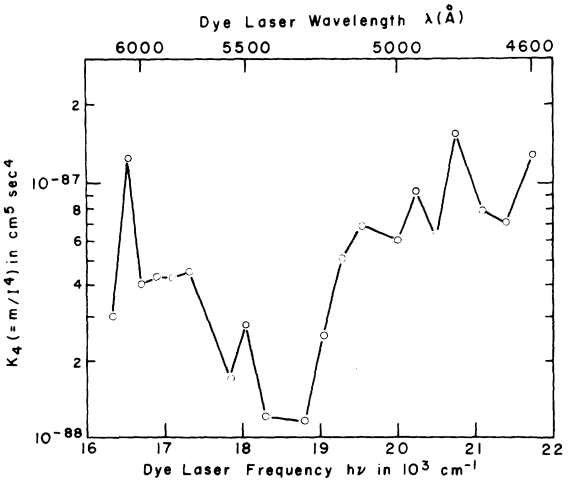

FIG. 8. Energy dependence of the generation coefficient for charge carriers via exciton collision ionization, $K_4(\nu)$ $(=m/I^4)$.

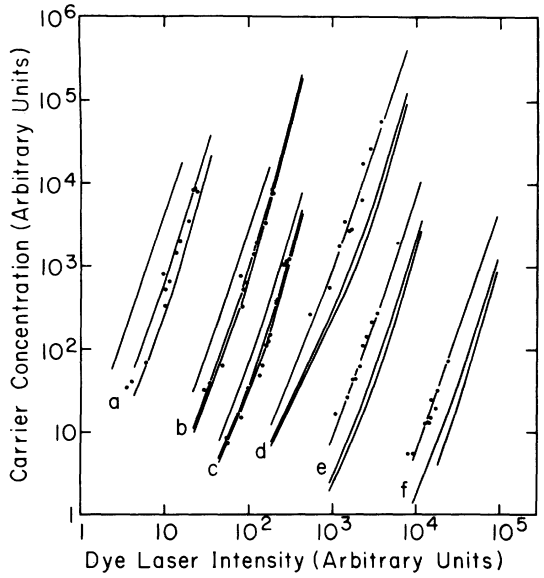

FIG. 9. Carrier concentration vs laser intensity (in region II) for the following wavelengths: (a) 5990 Å; (b) 6050 Å; (c) 6120 Å; (d) 4810 Å; (e) 4930 Å; (f) 5000 Å. The three solid curves are the analysis of the experimental data [using Eq. (7)], where for each energy we use three different values of $K_3(0, K_3', 10K_3')$. The value of $K_3'(\nu)$ was chosen assuming that $\sigma_p(\nu)$ for $\nu \geq 16300$ cm^{-1} is energy independent and thus $K_3(\nu) \alpha \sigma_2^F(\nu)$. Using the experimental value of $K_3(\nu = 16300)$ we take $K_3'(\nu) = 1.3 \times 10^{-63} \sigma_2^F(\nu)/\sigma_2^F(\nu = 16300)$.

the low intensity region. In Fig. 6 we display the energy dependence of the two-photon generation coefficient together with the two-photon-absorption cross sections previously reported by us.[29] For $2h\nu < 32500$ cm^{-1} we did not observe any square intensity contribution and the lowest energy point on the $K_2(2\nu)$ curve provides an upper limit for this quantity derived from the K_4 value observed at $2h\nu = 32400$ cm^{-1} ($\lambda = 6160$ Å). Also, within this range we were unable to observe the $m \propto I^2$ contribution (in the intensity range employed by us), at few energies, and again only an upper limit for K_2 could then be provided from the $K_4(2\nu)$ data. The $K_4(2\nu)$ values were evaluated from the high-intensity region of Fig. 5(II) and are summarized in Fig. 8. We have subsequently utilized Eq. (7) to obtain the best fit for $K_3(\nu)$. In Fig. 9 we display the analysis of our experimental data in region II, where for each energy we present three curves corresponding to different values of K_3 demonstrating the sensitivity of the m-vs-I dependence to the exciton photoionization coefficient. From the best fit at every energy, utilizing the $K_2(\nu)$ and $K_4(2\nu)$ data of Figs. 6 and 8, we obtain the energy dependence of $K_3(\nu)$ which is portrayed in Fig. 7. Several comments on these data (Figs. 6–8) are now in order.

(a) In region II ($2h\nu = 32500$–43500 cm^{-1}) all three charge-generation processes are observed simultaneously. The experimental data presented herein provide us with detailed quantitative information regarding the energy dependence of the charge-carrier generation coefficients.

(b) The onset of a finite $K_2(\nu)$ coefficient provides us with a quantitative estimate of the direct onset to the conduction band. From Fig. 6 we obtain $E_g = 32600 \pm 300$ cm^{-1} $= 4.08 \pm 0.04$ eV. This value is consistent with previous estimates[5,7–9] of $E_g = 3.9 \pm 0.2$ eV from one-photon experiments; however, it is obviously more accurate.

(c) The absolute values of K_2 are smaller (by a factor of ~10) than reported by Strome[19] and by Kepler.[6] At 5300 Å we get $K_2 = 7 \times 10^{-33}$ cm sec as compared with Strome's value $K_2 = 2 \times 10^{-31}$ cm sec at 5250 Å and with Kepler's result $K_2 = 1 \times 10^{-31}$ cm sec at 5300 Å. A careful examination of Fig. 6 (Ref. 6) and of Fig. 1 (Ref. 19) reveals a complex superlinear carrier-concentration dependence on the incident light intensity. There is an indication for a fourth-power dependence for high light intensities ($I > 3 \times 10^{23}$ photon cm^{-2} sec^{-1}) and a square dependence at lower intensities ($I = 10^{22}$–10^{23} cm^{-2} sec^{-1}). The value of K_2 (Fig. 6, Ref. 6) calculated

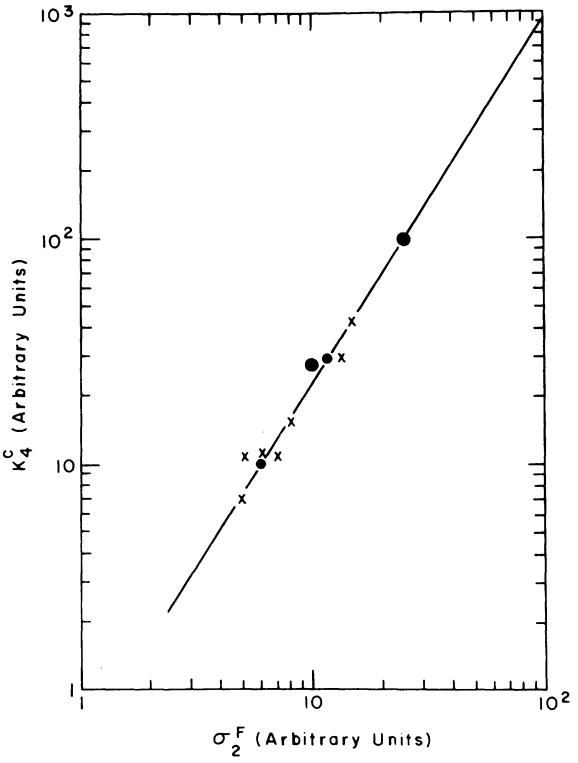

FIG. 10. Generation coefficients via exciton collision, K_4 vs σ_2^F, exhibit a square law dependence. The $\sigma_2^F \alpha \times (K_4)^{1/2}$ is found to hold for all the values in region II. ×, 4MU–$HClO_4$ dye laser, O, rhodamine 6G dye laser.

from the low-intensity region is 2.5×10^{-32} cm sec which is in reasonable agreement with our results.

(d) The direct observation of charge carrier generation via exciton collisions is consistent with the high two-photon absorption coefficients in this region.

(e) The generation coefficients via exciton collisions exhibit the $K_4(\nu)\propto[\sigma_2^F(2\nu)]^2$ dependence (see Fig. 10) over the whole energy region, as expected from Eq. (13), thus providing quantitative support to our interpretation. From Fig. 10 we get $\gamma_c=(4\pm2)\times10^{-12}$ cm^3 sec^{-1}. This value concurs with Braun's[15] analysis of one-photon photoconductivity data, which results in $\gamma_c\simeq10^{-12\pm0.4}$ cm^3 sec^{-1}.

C. Charge carrier generation from one-photon excited states

For weakly absorbed light the number of charge carriers generated from one-photon absorption below E_g is given by

$$m=K_1I^2\ , \tag{15}$$

$$K_1=K_1^P+K_1^c\ , \tag{16}$$

where the generation coefficient for exciton photoionization is

$$K_1^p=\sigma_p(\nu)\alpha\tau\beta^{-1}\ , \tag{17}$$

while the contribution of exciton collision is given by

$$K_1^c=\gamma_c\alpha^2\beta^{-2}\tau\ , \tag{18}$$

where α is the absorption coefficient and it was assumed that α^{-1} considerably exceeds the crystal thickness. The ratio of the generation coefficients is

$$b=K_1^p/K_1^c=\sigma_p(\nu)\beta/\gamma_c\alpha=10^{19}(\sigma_p/\alpha) \tag{19}$$

for reasonable values of $\sigma_p=10^{-20}$–10^{-19} cm^2, $b\simeq(10^{-1}/\alpha)$; thus for $\alpha<10^{-1}$ cm^{-1} charge-carrier generation via exciton photoionization dominates, as suggested by Kepler[6] and Strome,[19] while for $\alpha>1$ cm^{-1} exciton collision ionization will provide the major pathway for carrier generation, as suggested by Braun.[15]

From our experimental data (Fig. 5) we obtain $K_1=10^{-30}$ cm sec at 4500 Å and $K_1=8\times10^{-30}$ cm sec at 4400 Å. The absorption coefficients were obtained from Nakada's[56] data using Urbach's rule, which result in $\alpha=10^{-3}$ cm^{-1} at 4500 Å and $\alpha=8\times10^{-3}$ cm^{-1} at 4400 Å. Thus obviously in our region III, $K_1=K_1^p$, and we obtain a reasonable estimate for $\sigma_p(\nu)\simeq0.4\times10^{-19}$ cm^3 at these energies (see Sec. IV B).

D. Energy dependence of the cross sections for exciton photoionization

A fairly detailed information regarding the energy dependence of the cross sections for singlet exciton photoionization is obtained from our experimental data. The K_3 values obtained in region I together with Eq. (11) and the experimental values of σ_2^F, yield a direct measurement of $\sigma_p(\nu)$. The data K_1^P of region III together with the extrapolated values of α (see Sec. IV C) and Eq. (17) also result in reasonably accurate values of $\sigma_p(\nu)$ around 4400 Å. Finally, the $K_3(\nu)$ values obtained in region II (see Fig. 7) provide us with an approximate estimate of $\sigma_p(\nu)$ in this region. From Eq. (11) we have

$$\sigma_p(\nu)=K_3(\nu)\beta/\sigma_2^F(2\nu)L\tau\ . \tag{11a}$$

Equation (11a), together with the experimental values of σ_2^F which were independently obtained by us (see Fig. 6), can be utilized for the calculation of $\sigma_p(\nu)$. As at the onset of region II the two-photon-absorption cross sections exhibit a rapid variation with energy one can utilize an internal calibration procedure evaluating σ_2^F from the experimental value of $K_4(\nu)$. Thus from Eqs. (11) and (13) we have the simple result

$$\sigma_p(\nu)=\frac{K_3(\nu)}{[K_4(\nu)]^{1/2}}\left(\frac{\gamma_c}{\tau}\right)^{1/2}\ , \tag{20}$$

taking $\gamma_c=4\times10^{-12}$ cm^3 sec^{-1} obtained in Sec. IV B. The photoionization cross section evaluated from Eqs. (11a) and (20) are quite close; the latter are considered to be somewhat more reliable. The uncertainty of the σ_p values in region II (within a numerical factor of about 2) originates from the reliability of the curve fitting in Fig. 9. In Fig. 10 we present the energy dependence of $\sigma_p(\nu)$. The value $\sigma_p(14\,400\ \text{cm}^{-1})=4\times10^{-20}$ cm^2 is consistent with previous data[12,13] $\sigma_p=6\times10^{-20}$ cm^2 and $\sigma_p=2\times10^{-19}$ cm^2 reported at this energy.

The $\sigma_p(\nu)$ values correspond to the cross sections for one-photon-induced charge-carrier generation at the energy $\bar{E}=h\nu+E(S_1)=h\nu+25\,000$ cm^{-1}. Thus our data (Fig. 11) correspond to the energy region $\bar{E}=39\,400-48\,000$ cm^{-1}, which is located well above E_g. It should be pointed out that the term "photoionization cross sections" for $\sigma_p(\nu)$ is somewhat misleading, as charge-carrier generation resulting from excitation of S_1 should be again interpreted in terms of residual autoionization yield of metastable excitons (i.e., charge carriers produced by autoionization which subsequently escape genimate recombination) located at $\bar{E}$. Thus $\sigma_p(\nu)$ should be recast in terms of a product of one photon absorption coefficient $\sigma_1(\nu)$ from S_1 to a metastable state at $\bar{E}$ and the residual autoionization efficiency $\eta(\bar{E})$ at this energy, i.e. $\sigma_p(\nu)=\sigma_1(\nu)\times\eta(\bar{E})$. The one-photon-absorption cross sections $\sigma_1(\nu)$ correspond to transitions between excited electronic states. As the initial state involves the Frenkel excitons originating from the $^1B_{2u}$ molecular excited state, the final zero order states which

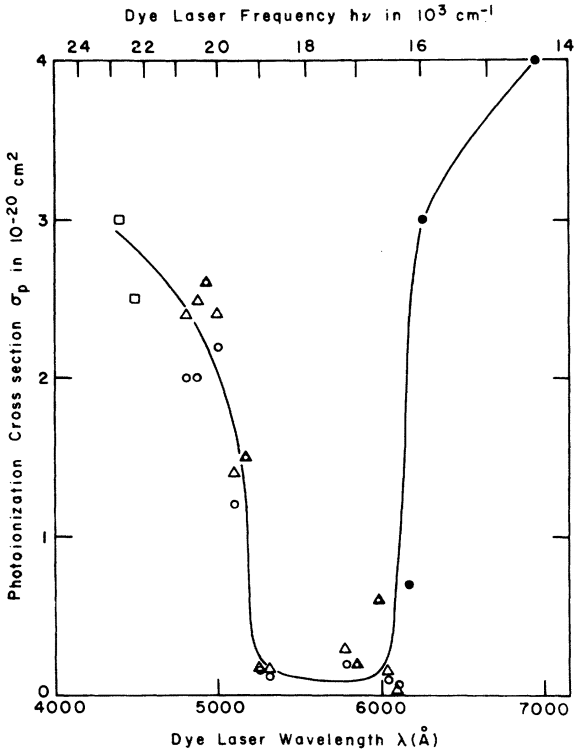

FIG. 11. Energy dependence of $\sigma_p(\nu)$. ●, obtained from region I [Fig. 5(I)], where K_3^c yield a direct measurement of $\sigma_p(\nu)$; ○, obtained from Eq. (11a) using the $K_3(\nu)$ values and σ_2^F in region II [Fig. 5(II)]; △, obtained from Eq. (20) using the $K_3(\nu)$ and $K_4(\nu)$ values in region II [Fig. 5(II)]; □, obtained from region III [Fig. 5(III)] together with the extrapolated values of one photon absorption cross section around 4400 Å.

carry oscillator strength from $^1B_{2u}$ will correspond to even parity Frenkel excitons which have their parentage in g-type molecular states. Transitions between excited molecular states of the anthracene molecule were studied[58] only for final states at $\overline{E} > 48\,000$ cm^{-1} and these data are not useful for us. Nanosecond flash photolysis studies of crystalline anthracene will result in a determination of $\sigma_1(\nu)$ leading to the energy dependence of $\eta(\overline{E})$.

E. Efficiency of exciton collision ionization

We can now provide a reliable estimate of the efficiency η_s for exciton collision ionization which corresponds to the residual autoionization yield of a metastable exciton produced at 49 000 cm^{-1} by collisions of S_1 excitons. Following previous discussions $\eta_s = \gamma_c/\gamma_s$. Here $\gamma_s = (6 \pm 2) \times 10^{-8}$ cm^{-3} sec^{-1} represents the rate of exciton collisions in this system. Utilizing the value $\gamma_c = 4 \times 10^{-12}$ cm^3 sec^{-1} obtained herein we get $\eta_s = (7 \pm 4) \times 10^{-5}$, which is quite consistent with previous guesses[7] and with Braun's[15] estimate from one-photon data.

V. AUTOIONIZATION EFFICIENCY OF METASTABLE EXCITONS

The experimental results for the energy dependence of $K_2(\nu)$ (Fig. 6) result in detailed information regarding the residual autoionization yield $\eta(E)$ of metastable excitons in the energy range 32 000–43 500 cm^{-1}. The residual autoionization efficiency at the energy $E = 2h\nu$ monitors the yield of charge carriers produced via autoionization and which manages to escape geminate recombination is obtained from Eqs. (5), (6), and (8):

$$\eta(E) = \frac{\sigma_2^c(\nu)}{\sigma_2^F(\nu)} = \frac{K_2(\nu)}{L\sigma_2^F(\nu)\pi} . \tag{21}$$

We can utilize the experimental data of $K_2(\nu)$ together with the cross sections for two-photon absorption determined independently[29] to evaluate $\eta(\nu)$ at different energies. Alternatively we can make use of an internal calibration procedure and evaluate $\sigma_2^F(\nu)$ from the $K_4(\nu)$ values. Making use of Eqs. (21) and (13) we then have

$$\eta(E) = \frac{K_2(\nu)}{[K_4(\nu)]^{1/2}} \left(\frac{\gamma_c}{\tau}\right)^{1/2} . \tag{22}$$

Equation (22) is more accurate than Eq. (21), as any uncertainty in the absolute determination of the light intensity does not come in while the accuracy in the determination of the absolute determination of the charge carrier concentration comes in as $m^{1/2}$. The energy dependence of $\eta(E)$ obtained from Eq. (21) together with the experimental σ_2^F values and from Eq. (22) taking $\gamma_c = 4 \times 10^{-12}$ cm^3 sec is portrayed in Fig. 12. From these results we arive at the following conclusion.

(a) The absolute experimental values of $\eta(E) \sim 10^{-5}$ obtained from two-photon studies in the energy region studied herein are consistent with previous

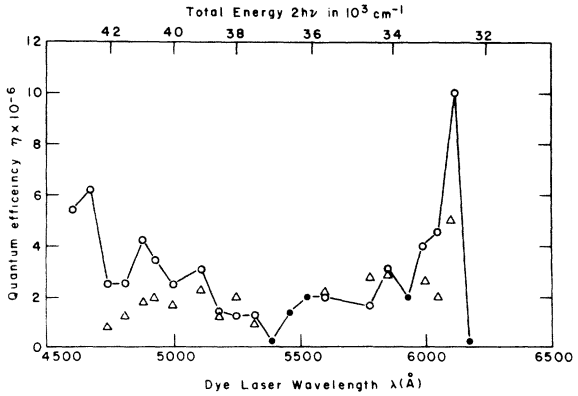

FIG. 12. Energy dependence of $\eta(E)$. △, obtained from Eq. (21) together with the experimental σ_2^F values; ○, obtained from Eq. (22) together with the experimental K_2^c and K_4^c values; ●, upper limit for $\eta(E)$ using the upper limit of K_2^c.

estimates of quantum yields[6-9,17] for carrier production from one-photon spectroscopy where the maximum value (at 2780 Å) was reported to be $\sim 10^{-4}$ (Ref. 7) and with Kepler's[6] estimate $\sigma_2^c/\sigma_2^F \sim 10^{-4}$ at 2.35 eV. The present data are, of course, much more extensive. Thus, in the entire energy region [see Eqs. (5) and (6)] $\exp(-\lambda/R_0)J(E)/W(E) \sim 10^{-5}$. As the attentuation factor, Eq. (6) is $\exp(-\lambda/R_0) \simeq 0.1$, we get $J(E)/W(E) \sim 10^{-4}$. The dominating role of the intramolecular nonradiative decay channel in the decay of metastable excitons in organic crystals has been previously discussed in relation to collision ionization[16,17] and one photon intrinsic photoconductivity.[18] The present data provide detailed information regarding the "fine structure" of the energy dependence of $\eta(E)$.

(b) The experimental yield $\eta(E) = 4\times10^{-6}$ at the higher energy $E = 42\,000$ cm^{-1} is somewhat lower than the value $\eta_s = (7\pm4)\times10^{-5}$ for the residual autoionization efficiency of a metastable exciton at 49 000 cm^{-1} produced by exciton collisions (see Sec. IV E).

(c) The sharp rise of $\eta(E)$ [and of $K_2(\nu)$] by at least one order of magnitude around $E = 32\,600$ cm^{-1} attributed by us to the onset of the conduction band. More precisely, this sharp rise corresponds to the energy of the bottom of the lowest vibronic component of the first conduction band, while the hole is located at the bottom of the lowest vibronic component of the highest valence band. This sharp rise of $\eta(E)$ obtained from the present two-photon experiments is in contrast with the one-photon photoconductivity yield curves which exhibit a gradual increase above E_g.[7] In view of the difficulties inherent in the one-photon data due to surface effects near the electrode contacts, we believe that our data are more reliable.

(d) The two-photon yield curve exhibits a gross structure which reveals two high efficiency regions peaked around 34 000 cm^{-1} and at about 42 000 cm^{-1}, which are separated by a minimum at 365 000 cm^{-1}. Each of these "bands" in $\eta(E)$ can be attributed to a different electronic configuration of both the valence and the conduction band, spanning all the separate vibronic components. The separation between the peaks ~ 8000 cm^{-1} is consistent with the separation between the one-photon photoconductivity peaks (9000 cm^{-1}).[9,18] On the basis of photoemission studies of Vilesov *et al.*[44] and of theoretical molecular levels calculations, Geacintov and Pope[9] have assigned these two "bands" in one-photon photoconductivity to excitation from the first two valence bands, and the same interpretation applies to the gross structure of our two-photon yield curves.

(e) The low-energy region of the $\eta(E)$ curve (36 000–32 000 cm^{-1}) exhibits a structure where neighboring components are separated by about ~ 1000 cm^{-1}. This separation is interpreted in terms of the vibrational structure of the lowest conduction band. The spacing of ~ 1000 cm^{-1} is consistent with the vibrational frequency of the anthracene negative molecular ion. Thus our data exhibit the vibronic splitting of the lowest conduction band or of the highest valence band. Previously, some evidence for this vibronic splitting was obtained from charge injection studies.[39]

(f) The low-energy region is characterized by a sharp maximum around 32 600 cm^{-1} just above E_g (see Fig. 12). This interesting feature is reserved for a special discussion later.

VI. INFORMATION AND CONJECTURES REGARDING THE WEIGHTED DENSITY OF STATES

It is evident from Eq. (5) that the yield function $\eta(E)$ monitors the complex ratio $\exp[-\lambda/R_0(E)] \times |V_E|^2\rho(E)/W_E$ and thus provides only a rough measure of the weighted density of states. This problem is widely encountered in studies of optical properties of solids where one monitors the product of the weighted density of states by an optical transition moment and the latter is assumed to exhibit weak energy (and wave-vector) dependence.[59] In the present case a further complication originates from the attenuation factor due to geminate recombination, which is, luckily, weakly energy dependent. It is interesting at this point to inquire what kind of semiquantitative information can be obtained from the $\eta(E)$ curve, in particular with regard to its sharp onset and perhaps also concerning the sharp maximum at 32 600 cm^{-1}. For this purpose let us consider in some detail the weighted density of states[59]

$$\rho(E) = \sum_{\vec{k}} \sum_{V} \sum_{C} \sum_{\alpha} \sum_{\beta} \delta[E + E(V, \alpha, \vec{k}) - E(C, \beta, \vec{k})] , \tag{23}$$

where the index $V = 1, 2, \ldots$ labels the particular electronic valence band (referring to the state of the hole), the index $C = 1, 2, \ldots$ refers to the electronic conduction band (in terms of the electronic state of the electron, α and β are the vibrational quantum numbers of the electron and hole bands, respectively, while $\vec{k}$ is the quasimomentum in the two bands. In Eq. (23) we have invoked just direct transitions. We can further rewrite Eq. (23) in terms of separate contributions from pairs of vibronic valence and conduction bands:

$$\rho(E) = \sum_{V\alpha} \sum_{C\beta} \rho_{V\alpha, C\beta}(E) \quad , \tag{24}$$

$$\rho_{V\alpha, C\beta}(E) = \sum_{\vec{k}} \delta[E + E(V, \alpha, \vec{k}) - E(C, \beta, \vec{k})] . \tag{25}$$

Thus, for example, the contribution to $\eta(E)$ and to $\rho(E)$ at lowest energy originates from $\rho_{10,10}(E)$, and in this system $E_g = E(C = 1, 00) - E(V = 1, 00)$.

Several universal features[59] of the partial

weighted density of state should be considered. Where

$$\nabla_{\vec{k}}[E(V,\alpha,\vec{k}) - E(C,\beta,\vec{k})] = 0\,, \tag{26}$$

we expect that $\rho_{V\alpha,C\beta}(E)$ will exhibit Van Hove type singularities. This will occur when either the (vibronic) valence band or the (vibronic) conduction band is characterized by such a singulraity. Now in a narrow energy region just above E_g we expect $\eta(E) \propto \rho_{10,10}(E)$ and $\eta(E)$ might exhibit the singularities in the vibronic densities of states. We thus propose that the energy dependence of $\eta(E)$, at least near threshold, will provide new information regarding the lowest weighted density of states in this system.

From theoretical calculations it is evident that the band structure of the lowest excess electron and hole bands in crystalline anthracene is dominated by two-dimensional interactions in the *ab* crystal plane. Thus the resulting densities of states in the lowest conduction band and in the highest valence bands will be two dimensional. Thus the weighted density of states $\rho_{1\alpha,1\beta}(E)$ (and possibly also the higher partial densities of states for $V>1$ and $C>1$) will exhibit the two-dimensional Van Hove singularities, which are discontinuities at extremum (minimum or maximum) points and logarithmic singularities at saddle points. Obviously, all these singularities will be somewhat smeared out in real life due to coupling with intermolecular phonons, and in view of the finite spectral resolution employed in such experiments.

We propose that the sharp onset of $\eta(E)$ at E_g monitors the minimum of $\rho_{10,10}(E)$ which should indeed be characterized by a discontinuity in a two dimensional band structure. We further speculate that the sharp maximum at $E = 32\,600$ cm^{-1} may originate from a logarithmic singularity in this lowest components $\rho_{10,10}(E)$, as expected for a two-dimensional density of states. The last tentative conclusion should be taken with a grain of salt as the spectral resolution (of the dye laser) employed by us (~ 150 cm^{-1}) is relatively low and the extension of the present measurements at higher resolution will be desirable.

When the energy is somewhat further increased the $\eta(E)$ curve monitors the weighted densities of states $\rho_{1\alpha,1\beta}(E)$, which are spaced by the totally symmetric vibrational frequency $\hbar w$, which is taken to be approximately equal for the molecular positive and negative ions. As we were able to resolve steplike structure above E_g with spacing $\hbar w \sim 1000$ cm^{-1} we conclude that the width Δ of each partial weighted density of states function $\rho_{1\alpha,1\beta}(E)$ is of the order of $\Delta \sim \hbar w \sim 1000$ cm^{-1}. Thus the observed lowest vibronic bands are indeed narrow, as expected on the basis of the theoretical calculations.

When the energy is further increased above 37 000 cm^{-1} $\eta(E)$ exhibits a second broad maximum corresponding to the contributions of $\rho_{V\alpha,C\beta}(E)$ (with $C>1$ or $V>1$, or both). We note that the sharp maximum is exhibited only for $\rho_{10,10}(E)$ and not for $\rho_{1\alpha,1\beta}(E)$ ($\alpha, \beta > 1$) and that for $\rho_{V\alpha,C\beta}(E)$ (V or $C>1$) the structure is almost washed out and even the vibronic components cannot be any more well resolved.

We have argued in Sec. II that higher vibronic components of the lowest conduction band and lower vibronic components of the valence band will relax by vibrational relaxation so that the fine structure of the density of states will be partially smeared out just retaining the steplike structure of different vibronic components $\rho_{1\alpha,1\beta}$. At even higher energies congestion of different vibronic states corresponding to various electronic configurations together with nonradiative electronic relaxation to lower bands and Auger type processes (see Sec. II) will completely smear out all structure in $\eta(E)$. This does not, of course, imply the existence of a broad conduction band as in simple insulators like alkali halides or solid rare gases[59] but rather loss of structure due to overlapping broadened components.

To conclude this discussion we would like to point out that the present approach to the understanding of autoionization cross sections of metastable excitons (induced by two photon absorption) in molecular crystals or organic molecules is entirely different from the conventional two-photon spectroscopy in these solids. While the interpretation[27-29] of the $\sigma_2^F(E)$-vs-E curves rests on the assignment of Frenkel type (zero order) g states the study of the $\eta(E)$-vs-E curves provides information regarding the weighted density of states. The basic philosophy in the interpretation of the autoionization yields is also somewhat different from the related studies of photoconductivity of simple insulators as in our case the role of the intramolecular non radiative dissipative channel is crucial.

[1] F. Gutman and L. E. Lyons, *Organic Semiconductors* (Wiley, New York, 1967).

[2] H. Helfrisch, in *Physics and Chemistry of the Organic Solid State*, edited by D. Fox, M. M. Labes, and A. Weissberger (Interscience, New York, 1967), Vol. III Chap. 1.

[3] O. H. Leblanc, Ref. 2, Vol. III, Chap. 3.

[4] M. Silver, *Conductivity in Low Mobility Materials*, edited by N. Klein, D. S. Tanhauser, and M. Pollak (Taylor and Francis, London, 1971), p. 347.

[5] M. Pope and H. Kallman, Disc. Faraday Soc. 51, 7 (1971).

[6]R. G. Kepler, in *Proceedings of Second International Symposium on Organic Solid Chemistry, Rehovot, Israel* (Butterworth, London, 1971).
[7]G. Castro and R. Hornig, J. Chem. Phys. 42, 1459 (1965).
[8]R. F. Chaiken and D. R. Kearns, J. Chem. Phys. 45, 3966 (1966).
[9]N. E. Geacintov and M. Pope, J. Chem. Phys. 45, 3884 (1966).
[10]See, for example, J. M. Worlock, in *Laser Handbook*, edited by F. T. Arecchi and E. O. Schulz-Dubois (North Holland, Amsterdam, 1972).
[11]S. I. Choi, J. Chem. Phys. 40, 1691 (1964).
[12]R. G. Kepler, Phys. Rev. Letters 18, 951 (1967).
[13]E. Courtens, A. Bergman and J. Jortner, Phys. Rev. 156, 948 (1967).
[14]S. I. Choi and S. A. Rice, J. Chem. Phys. 38, 366 (1963).
[15]L. Braun, Phys. Rev. Letters 21, 215 (1968).
[16]S. I. Choi, Phys. Rev. Letters 19, 358 (1967).
[17](a) J. Jortner, Phys. Rev. Letters 20, 244 (1968). (b) J. Jortner and M. Bixon, Mol. Cryst. 9, 231 (1969).
[18]N. Geacintov and M. Pope, J. Chem. Phys. 50, 814 (1969).
[19]G. Strome, Phys. Rev. Letters 20, 3 (1968).
[20]R. G. Kepler, Appl. Opt. Suppl. 3, 25 (1969).
[21]A. S. Davydov, *Theory of Molecular Excitons* (Plenum, New York, 1970).
[22]G. W. Robinson, Ann. Rev. Phys. Chem. 21, 429 (1970).
[23]S. Singh, W. J. Jones, W. Siebrand, R. P. Stoicheff, and W. G. Schneider, J. Chem. Phys. 42, 330 (1965).
[24]J. L. Hall, P. A. Jenning, and R. M. McLintock, Phys. Rev. Lett. 11, 364 (1963).
[25]A. Bergman, M. Levine, and J. Jortner, Phys. Rev. Lett. 18, 593 (1966).
[26]D. Frohlich and H. Mahr, Phys. Rev. Lett. 18, 593 (1966).
[27]J. P. Hernandez and A. Gold, Phys. Rev. 156, 26 (1967).
[28]I. Webman and J. Jortner, J. Chem. Phys. 50, 2706 (1969).
[29]A. Bergman and J. Jortner, Chem. Phys. Letters 15, 309 (1972).
[30]W. T. Simpson and D. L. Peterson, J. Chem. Phys. 26, 588 (1951).
[31](a) L. E. Lyons, J. Chem. Soc. 5001 (1951); (b) H. Sternlicht and M. H. McConnel, J. Chem. Phys. 35, 1793 (1961).
[32]R. S. Berry, J. Jortner, J. C. Mackie, E. S. Pysh, and S. A. Rice, J. Chem. Phys. 42, 1535 (1965).
[33]S. I. Choi, J. Jortner, S. A. Rice, and R. Silbey, J. Chem. Phys. 41, 3294 (1964).
[34]J. P. Hernandez and S. I. Choi, J. Chem. Phys. 50, 1524 (1969).
[35]M. Pope and J. Burgos, Mol. Cryst. 1, 305 (1966).
[36]M. Pope, H. Kleinman, and J. Giachino, J. Chem. Phys. 42, 2540 (1965).
[37]G. T. Pott and D. F. Williams, J. Chem. Phys. 51, 203 (1969).
[38]D. Haarer and G. Castro, Chem. Phys. Lett. 12, 277 (1971).
[39](a) G. Vaubel and H. Baessler, Phys. Status Solidi 26, 599 (1968). (b) Phys. Lett. A 27, 328 (1968).
[40]O. H. Leblanc, J. Chem. Phys. 35, 1275 (1960).
[41]J. L. Katz, S. I. Choi, S. A. Rice, and J. Jortner, J. Chem. Phys. 39, 1683 (1963).
[42]R. Silbey, J. Jortner, S. A. Rice, and M. T. Vala, J. Chem. Phys. 42, 733 (1965).
[43]R. M. Glaeser and R. S. Berry, J. Chem. Phys. 44, 3797 (1966).
[44]F. I. Vilesov, A. A. Zagrubskii, and D. D. Garbuzov, Sov. Phys. Solid State 5, 1460 (1964).
[45]J. Dresner, J. Chem. Phys. 52, 6343 (1970).
[46]See, for example, J. Jortner, Pure and Applied Chemistry 24, 167 (1970).
[47]The previous treatment (Ref. 18) using the techniques of Ref. 17 has to be slightly modified, as outlined herein.
[48]U. Fano, Phys. Rev. 124, 1866 (1961).
[49]S. D. Druger, Chem. Phys. Lett. 17, 603 (1972).
[50](a) A. Bergman, M. Levine, and J. Jortner, Phys. Rev. Lett. 18, 593 (1966); (b) N. A. Tolstoi and A. V. Abramov, Sov. Phys. Solid State 9, 255 (1967); (c) A. Bergman, D. Bergman, and J. Jortner, Israel J. Chem. 10, 471 (1972); (d) the rate reported in Ref. 50, $\frac{1}{2}\gamma_s$, corresponds to the dominating decay made of a pair of singlet excitons involves the production of a single S_1 exciton via internal conversion.
[51](a) R. G. Kepler and F. N. Coppage, Phys. Rev. 151, 610 (1966); (b) R. H. Batt, C. L. Braun, and J. F. Hornig, J. Chem. Phys. 49, 1967 (1968); (c) R. H. Batt, C. L. Braun, and J. F. Hornig, Appl. Opt. Suppl. 3, 20 (1969); (d) N. E. Geacintov and M. Pope, in *Proceedings of the Third International Photoconductivity Conference, Stanford*, 1969, edited by E. M. Pell (Pergamon, New York, 1971), p. 289. (e) R. R. Chance and C. L. Braun, J. Chem. Phys. 59, 2269 (1973); (f) L. Onsager, Phys. Rev. 54, 599 (1934).
[52]M. Silver, D. Olness, M. Swicord, and R. C. Jarnagin, Phys. Rev. Lett. 10, 12 (1963).
[53](a) C. V. Shank, A. Dienes, A. M. Trozzolo, and J. A. Myer, Appl. Phys. Lett. 10, 405 (1970). (b) A. Dienes, C. V. Shank, and A. M. Trozzolo, Appl. Phys. Lett. 5, 189 (1970). (c) C. V. Shank, A. Dienes, and W. T. Silfvast, Appl. Phys. Lett. 7, 307 (1970).
[54]A. Bergman, R. David, and J. Jortner, Opt. Commun. 4, 431 (1972).
[55] An alternative mechanism which will also result in a $m = K_2^T I^2$ intensity dependence can originate from photoionization of one-photon-excited triplet excitons, i.e., $S_0 \rightarrow T_1 \rightarrow e + h$. The generation coefficient K_2^T for charge carrier production by this mechanism is given by $K_2^T = \alpha_T \gamma_p^T \tau^2$. $\alpha_T \simeq 10^{-4}$ cm^{-1} is the $S_0 \rightarrow T_1$ absorption coefficient [P. Avakian and R. Merrifield, Mol. Cryst. 5, 37 (1968)]. $\gamma_p^T \simeq 5 \times 10^{-22}$ cm^{-2} at 5250 Å according to Strome (Ref. 19); this value seems to be more reliable than $\gamma_p^T \simeq 4 \times 10^{-21}$ cm^2 due to Holtzman *et al.* [P. Holtzman, R. Morris, and R. C. Jarnagin, Phys. Rev. Lett. 19, 506 (1967)]. Finally $\tau = 10^{-8}$ sec is the pulse duration. Thus $K_2^T \simeq 10^{-41}$ cm sec^{-2}. The experimental data for the two-photon charge-carrier generalization coefficients (see Fig. 6) exceed 10^{-40} cm sec^{-2} except at the low-energy onset and at a single point at $2h\vartheta = 3700$ cm^{-1}. This provides an *a posteriori* argument that the contribution of triplet-exciton photoionization process is small.
[56]I. Nakada, J. Phys. Soc. of Japan 20, 346 (1965).
[57]M. Schott, Phys. Lett. 23, 92 (1966).
[58]D. S. Kliger and A. C. Albrecht, J. Chem. Phys. 53, 4059 (1970).
[59]J. C. Phillips, Solid State Phys. 18, 55 (1966).